Proc. Natl. Acad. Sci. USA
Vol. 79, pp. 3754–3758, June 1982
Biophysics

Electrostatic potential molecular surfaces

(nucleic acids/proteins/drug–nucleic acid interactions/protein–ligand interactions)

PAUL K. WEINER, ROBERT LANGRIDGE, JEFFREY M. BLANEY, RONALD SCHAEFER, AND PETER A. KOLLMAN

Department of Pharmaceutical Chemistry, School of Pharmacy and School of Medicine, University of California, San Francisco, California 94143

Communicated by Robert G. Parr, January 20, 1982

ABSTRACT **Color-coded computer graphics representations of the electrostatic potentials of trypsin, trypsin-inhibitor, prealbumin and its thyroxine complex, fragments of double-helical DNA, and a netropsin–DNA complex illustrate the electrostatic and topographic complementarity in macromolecule–ligand interactions. This approach is powerful in revealing intermolecular specificity and shows promise of having predictive value in drug design.**

The electrostatic potential is a powerful tool that has provided insights into intermolecular association and molecular properties of small molecules (1), actions of drug molecules and their analogs (2), the biological function of hemoglobin (3), and enzyme catalysis (4). We thought that, given the electrostatic potentials of both a ligand and its receptor, much greater progress might be made in the "rational design" of the optimal ligand (5–7). Subsequent studies of the electrostatic potentials of macromolecules (8–10) demonstrate the feasibility of this approach, but there has been no satisfactory way to represent the electrostatic potential in a way useful for understanding electrostatic complementarity. This problem is effectively solved by displaying the electrostatic potential molecular surface with a real-time interactive color graphics facility (11) using the molecular surface definition of Richards (12) and the algorithm developed by M. Connolly.*

METHODS

At van der Waals distances and beyond, the simple classical formula reproduces the quantum mechanically calculated electrostatic potential quite well (5–7).

The classical formula for the electrostatic potential V at a point F for a system of charges q_i at points r_i in a medium of dielectric constant ε is given by:

$$V = \sum_i \frac{q_i}{\varepsilon |r_i - F|} .$$

We use a distance-dependent dielectric constant (13, 14), $\varepsilon = |r_i - F|$, in these calculations. This model has been successfully applied in energy refinement of complex molecules and uses Mulliken net atomic charges obtained from STO-3G *ab initio* and CNDO/2 calculations to represent q_i (15–18).

What should one use for the ionization state of exposed acidic and basic residues (9)? An assumption that all residues are in their predominant state of ionization in aqueous solution at pH 7 exaggerates the importance of the charged residues, whereas an assumption of neutrality ignores the effects of the charged groups. Here we adopt the following compromise: for protein calculations the charges were retained, and for nucleic acids we either explicitly included counterions or neutralized the phosphate charges.

The molecular surfaces for each structure were calculated from x-ray and energy-refined coordinates (19–21) by using the program MS (22). The electrostatic potential was calculated 1.4 Å along the surface normal vector from a given molecular surface point and represented at the surface point itself. We calculated the contribution of each atom within 20 Å of the electrostatic potential point F and used the method of neutral spheres (23, 24), which corrects for dipoles split by the finite cutoff radius by adding an additional interaction (at that radius) to ensure that the net charge inside the sphere is zero. The surfaces were displayed at the University of California (San Francisco) Computer Graphics Laboratory with the display program HANDLE (written by M. Connolly).

RESULTS

Trypsin–Trypsin Inhibitor. First we consider the prototype protein–protein interaction of trypsin and bovine pancreatic trypsin inhibitor (BPTI) (25). There is a large negative pocket (due to Asp-189) in trypsin that is the binding pocket for the positively charged Lys-15 on the lower right of BPTI (Fig. 1). The predominance of positive charge on the lower half of BPTI was unexpected. In this region, the electrostatic potential is almost entirely positive, whereas the top half has regions of negative potential. This combination of attractive and repulsive forces may help guide BPTI into the correct position for binding before actually contacting the active site. This electrostatic complementarity is not evident from a surface that is color coded by atom type (Fig. 1 *Lower*). The driving forces for the binding of BPTI to trypsin are thus a complementary surface fit and electrostatic complementarity (26).

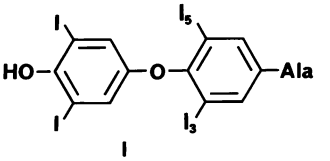

Prealbumin and Thyroid Hormones. Human plasma thyroxine-binding prealbumin is the first fully characterized hormone-binding protein. The residues in the binding site form close contacts with both aromatic rings of thyroxine (I); the carboxyl and ammonium groups of the thyroid hormone are associated by ion pairing with the Lys-15 and the Glu-54 residues in the mouth of the site. The structure of prealbumin led Blake and Oatley to conclude that its twisted β-sheet structure seemed of the correct radius to bind a DNA double helix (27). Attempts to find evidence for the binding of DNA to prealbumin have been unsuccessful (28).

The electrostatic potential molecular surface of prealbumin

The publication costs of this article were defrayed in part by page charge payment. This article must therefore be hereby marked "*advertisement*" in accordance with 18 U. S. C. §1734 solely to indicate this fact.

Abbreviations: BPTI, bovine pancreatic trypsin inhibitor; T4, L-thyroxine.

* A computer-generated film illustrating these results was shown at the Conference on Biomolecular Stereodynamics, Albany, NY, April 1981.

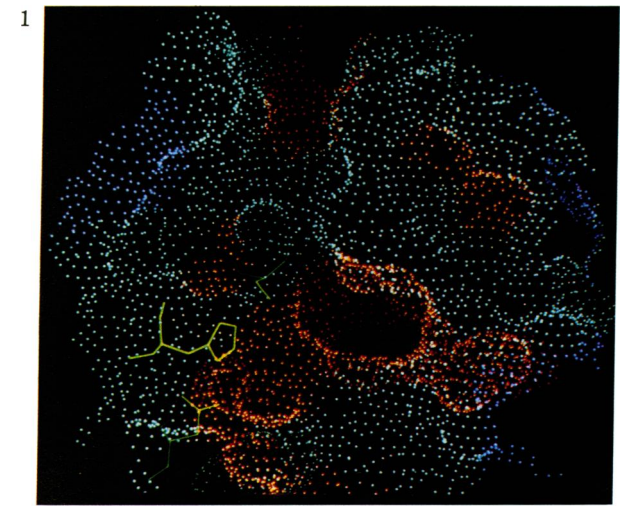

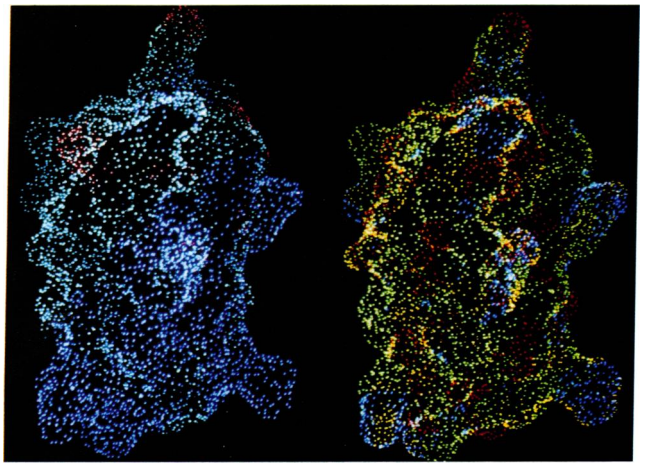

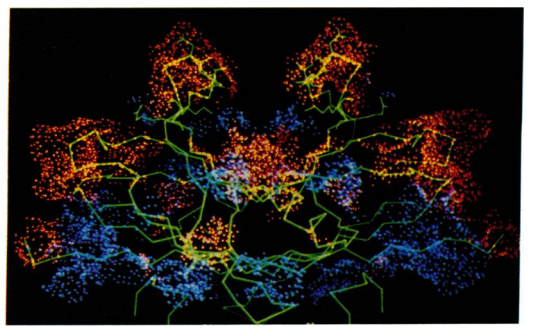

FIG. 1. (*Upper*) Electrostatic potential at the surface of the active site of trypsin. The binding site crevice on the surface begins at the top center and extends to the red depression in the middle of the picture. Contour levels: red, $V < -10$ kcal/mol (1 cal = 4.184 J); green, -10 kcal/mol $< V < +10$ kcal/mol; blue, $V > +10$ kcal/mol. (*Lower*) Molecular surface of BPTI. The lower part of the inhibitor fits into the binding site crevice of trypsin, with the "knob" at the lower right fitting into the red hole in the trypsin binding site. Color coded by electrostatic potential (*Left*) with contour levels as in *Upper* and colored by atom type (*Right*): red, O; green, C; blue, N.

FIG. 2. Electrostatic potential around the prealbumin dimer, with the putative DNA-binding groove at the top and the thyroxine-binding sites at the lower left and right of the picture. Contour levels as in Fig. 1 *Upper* (only the red and blue surface are displayed, because of limitations of the picture system memory).

is shown in Fig. 2, with the putative binding site for DNA at the top of the figure and the thyroxine binding site below. The putative DNA-binding site is predominantly negative and therefore is not electrostatically complementary to DNA. The

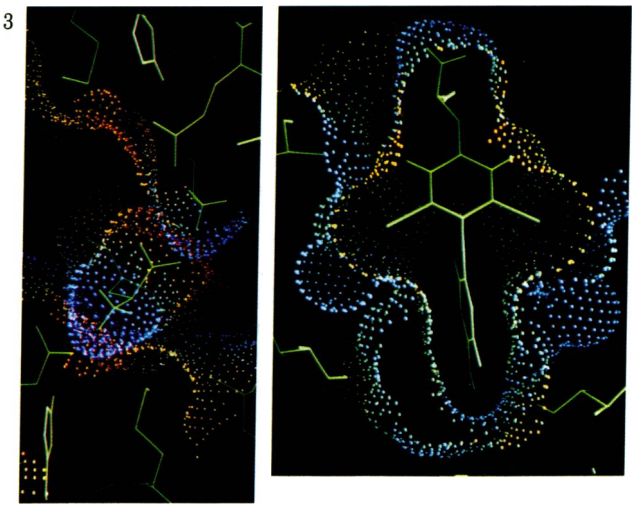

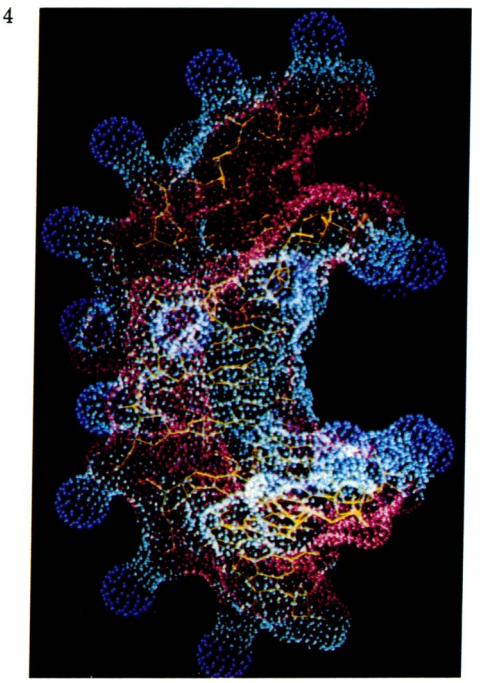

FIG. 3. (*Left*) Electrostatic potentials of the interacting, complementary molecular surfaces of the amino acid moiety of T4 and the hormone-binding site of prealbumin in the region of Lys-15 and Glu-54. Contour levels: red, $V < -20$ kcal/mol; orange, -20 kcal/mol $< V < -10$ kcal/mol; green, -10 kcal/mol $< V < +10$ kcal/mol; light blue, $+10$ kcal/mol $< V < +20$ kcal/mol; dark blue, $V > +25$ kcal/mol. (*Right*) Cross section of the electrostatic potentials of the interacting molecular surfaces of T4 and prealbumin, showing the binding pockets for I-3 and I-5 of T4. Contours as in *Left*.

FIG. 4. Electrostatic potential surface of energy-refined d(C-G-C-G-A-A-T-T-C-G-C-T)$_2$ with Na^+ counterions on each phosphate. Contour levels as in Fig. 1. Note the very negative minor groove (top right) and the much less polar major groove (middle right).

thyroxine-binding site of prealbumin is predominantly positive, consistent with the observation (29) that the relative binding affinities to prealbumin of L-thyroxine (T4) and its des-amino and des-carboxy analogs are in the order: des-amino-T4 > T4 > des-carboxy-T4. Prealbumin has a strong affinity for retinol-binding protein (30) which increases with increasing ionic strength, suggesting that the association is hydrophobic. This association would be expected to take place on the broad bands of "neutral" surface on the exterior of prealbumin. However,

electrostatic complementarity may well come from the two negative "arms" of prealbumin near the putative DNA binding site which could interact with the predominantly positive NH_2 terminus of retinol-binding protein (31).

A "high-resolution" view (Fig. 3 *Left*) of the thyroid hormone binding site of prealbumin shows the electrostatic complementarity of the $-NH_3^+$ and $-COO^-$ groups of T4 to the Lys-15 and Glu-54 side chains. I-3 and I-5 of T4 are held by pockets lined with the side chains of hydrophobic residues, suggesting that high binding affinity to prealbumin would be retained upon replacement of I-3 and I-5 by alkyl groups of similar size and lipophilicity. However, the electrostatic potential at the surface of the pockets (Fig. 3 *Right*) is slightly positive due to the influence of the nearby Lys-15 ammonium group. Thus, the pockets are both topographically and electrostatically complementary to the slightly negative surfaces of I-3 and I-5, consistent with experimental results (29) which show that 3,5-dihalo analogs have much higher binding affinities to prealbumin than 3,5-dialkyl analogs. The halogens contribute a negative potential to their surface which interacts favorably with the positive potential in the pockets, whereas the hydrogens of the alkyl groups are slightly positive and lead to a repulsive interaction with the pockets.

Nucleic Acids. The electrostatic potential of DNA depends on the way the charges on the phosphate groups are described. A full negative charge on each phosphate makes the surface potential completely negative. We thus consider two alternative representations of DNA.

The first representation of $d(C\text{-}G\text{-}C\text{-}G\text{-}A\text{-}A\text{-}T\text{-}T\text{-}C\text{-}G\text{-}C\text{-}G)_2$ is B-DNA with a Na^+ counterion placed along the bisector of each phosphate PO_2^- group, and then completely energy refined. The electrostatic potential molecular surface (Fig. 4) shows the remaining large negative potential in the minor groove, whereas the major groove is relatively neutral, consistent with the observation by Drew and Dickerson (32) of a more ordered water structure in the minor than in the major groove in the crystal structure of this molecule. Counterions damp the negative phosphate electrostatic potential predominantly in the major groove.

The second representation of the phosphate group neutralization is to decrease the charges on the phosphate oxygens so that the molecule becomes neutral. An examination of the major groove groups of a C·G base pair [C-4-NH_2 (δ^+), G-6-CO (δ^-), and G-N7 (δ^-)] indicated that this base pair should have a larger electrostatic potential gradient in the major groove than a T·A pair [T-4-CO (δ^-), A-6-NH_2 (δ^+), and A-N7 (δ^-)]. We expected and found a rather different pattern of electrostatic potentials for $d(C_6)\cdot d(G_6)$—for which one side of the groove should be negative and the other positive—than for $d(C\text{-}G\text{-}C\text{-}G\text{-}C\text{-}G)_2$—for which the pattern should alternate (Fig. 5 *Upper Left*).

The electrostatic potentials in the major grooves of $d(T\text{-}A\text{-}T\text{-}A\text{-}T\text{-}A)_2$ and $d(A_6)\cdot d(T_6)$ are shown in Fig. 5 *Lower Left*. For $d(T\text{-}A\text{-}T\text{-}A\text{-}T\text{-}A)_2$, the potential surface has two positive areas resulting from two adjacent A-6-NH_2 groups and one negative patch due to the intrastrand juxtaposition of two T C=O groups. For $d(A_6)\cdot d(T_6)$ the surface is green. $d(G_6)\cdot d(C_6)$ and $d(C\text{-}G\text{-}C\text{-}G\text{-}C\text{-}G)_2$ show a much greater difference in their major groove electrostatic potentials because replacing G·C by C·G changes the "electrostatic polarity" from $--+$ to $+--$. In the A·T polymers, both A·T and T·A have polarity $-+-$.

The potential in the minor groove of $d(A_6)\cdot d(T_6)$ or $d(T\text{-}A\text{-}T\text{-}A\text{-}T\text{-}A)_2$ (Fig. 5 *Upper Right*) is entirely negative. The potential in the minor groove of $d(C\text{-}G\text{-}C\text{-}G\text{-}C\text{-}G)_2$ or $d(G_6)\cdot d(C_6)$ (Fig. 5 *Lower Right*) has negative areas but is not as negative as the A·T polymers, due to the guanine 2-NH_2 (δ^+) in the minor groove of C·G polymers. Unlike the A·T major groove, where a $-+-$ electrostatic pattern has virtually no negative potential as low as -4 kcal/mol, the G·C minor groove has large negative areas because of the contribution of phosphate oxygens to the negative potential in the narrow minor groove (Fig. 4).

With the neutralized phosphate representation, the minor groove in the region of the two $(C\text{-}G\text{-}C\text{-}G)_2$ fragments of $d(C\text{-}G\text{-}C\text{-}G\text{-}A\text{-}A\text{-}T\text{-}T\text{-}C\text{-}G\text{-}C\text{-}T)_2$ has negative and neutral areas similar to the potential for $d(C\text{-}G\text{-}C\text{-}G\text{-}C\text{-}G)_2$. In the region of $d(A\text{-}A\text{-}T\text{-}T)_2$, the minor groove potential is completely negative, as in $d(A_6)\cdot d(T_6)$ and $d(T\text{-}A\text{-}T\text{-}A\text{-}T\text{-}A)_2$. In the major groove, the electrostatic potential near the $(C\text{-}G\text{-}C\text{-}G)_2$ fragments has the alternating "diamond" pattern seen in $d(C\text{-}G\text{-}C\text{-}G\text{-}C\text{-}G)_2$ and the potential in the major groove near A-A-T-T is neutral except for the small positive patch due to the two A-6-NH_2 groups, just as was noted for $d(C\text{-}G\text{-}C\text{-}G\text{-}C\text{-}G)_2$ and $d(T\text{-}A\text{-}T\text{-}A\text{-}T\text{-}A)_2$. This may be an electrophilic site for the binding of *Eco*RI to its restriction site G-A-A-T-T-C (33). Thus, the electrostatic potential of $d(C\text{-}G\text{-}C\text{-}G\text{-}A\text{-}A\text{-}T\text{-}T\text{-}C\text{-}G\text{-}C\text{-}G)_2$ is nearly the sum of the "local potentials" for $d(A_6)\cdot d(T_6)$, $d(T\text{-}A\text{-}T\text{-}A\text{-}T\text{-}A)_2$, and $d(C\text{-}G\text{-}C\text{-}G\text{-}C\text{-}G)_2$, with one exception. This is a negative region where the thymine-C4 carbonyl group reinforces the negative potential of the guanine-C6 carbonyl on the opposite strand at the junction of the C·G and A·T regions, similar to the juxtaposition mentioned above for the two adenine-6-NH_2 groups.

In summary, there are two primary contributors to the electrostatic patterns observed in the potentials of $d(G\text{-}C\text{-}G\text{-}C\text{-}G\text{-}C)_2$, $d(G_6)\cdot d(C_6)$, $d(T\text{-}A\text{-}T\text{-}A\text{-}T\text{-}A)_2$, $d(A_6)\cdot d(T_6)$, and $d(C\text{-}G\text{-}C\text{-}G\text{-}A\text{-}A\text{-}T\text{-}T\text{-}C\text{-}G\text{-}C\text{-}G)_2$. The first contributor to large polarity is the intrinsic base pair potential, which is large for a G·C base pair ($--+$) and small for A·T($-+-$). This causes the dramatic differences between the potentials in the major groove for $d(G_6)\cdot d(C_6)$ and $d(A_6)\cdot d(T_6)$ (Fig. 5 *Upper* and *Lower Left*). The second main contributor is a nearest-neighbor interaction, which can either reinforce the intrinsic base pair potentials or decrease these potentials. For example, $d(C\text{-}G\text{-}C\text{-}G\text{-}C\text{-}G)_2$ has more neutral areas than does $d(G_6)\cdot d(C_6)$ because the neighboring base pair potentials $\mp = \pm$ somewhat cancel each other. In $d(A\text{-}T\text{-}A\text{-}T\text{-}A\text{-}T)_2$ the interstrand juxtaposition of two adenine NH_2 groups creates a positive region, whereas in $d(C\text{-}G\text{-}C\text{-}G\text{-}A\text{-}A\text{-}T\text{-}T\text{-}C\text{-}G\text{-}C\text{-}T)_2$ the interstrand juxtaposition of the G and T C=O groups creates a negative region. Using these principles, one can predict the nature of the major groove electrostatic potential for an arbitrary base sequence.

The different polarities of the C·G and A·T base pairs in the major groove may prove important in determining the way restriction endonucleases recognize specific patterns of base pairs in DNA (33). Of 213 known restriction endonucleases, there are 22 examples in which A can replace T in the recognition pattern but only 2 of G replacing C. These two G/C degeneracies occur in the sequence $G\text{-}G(\begin{smallmatrix}C\\G\end{smallmatrix})C\text{-}C$. These frequencies can be explained by the fact that the electrostatic patterns of the major grooves of $d(T\text{-}A\text{-}T\text{-}A\text{-}T\text{-}A)_2$ and $d(A_6)\cdot d(T_6)$ are more similar than those of $d(G\text{-}C\text{-}G\text{-}C\text{-}G\text{-}C)_2$ and $d(G_6)\cdot d(C_6)$. This, taken with the fact that the minor grooves of the above pairs look much the same, leads to the conclusion that it is the major groove that is important in restriction endonuclease recognition, in agreement with the results of methylation experiments (34).

In view of the recent x-ray structure of the *cro* protein (35), it is likely that the topography of the electrostatic potential in the major groove of DNA will be essential in understanding the basis for the sequence-specific recognition of DNA by this protein. The sequence (36) of the 17-base-pair OR3 site on bacteriophage λ, for which the *cro* protein has a high affinity, contains three consecutive G·C pairs at base pair locations 12–14. The related OR1 and OR2 sites, to which *cro* protein binds with

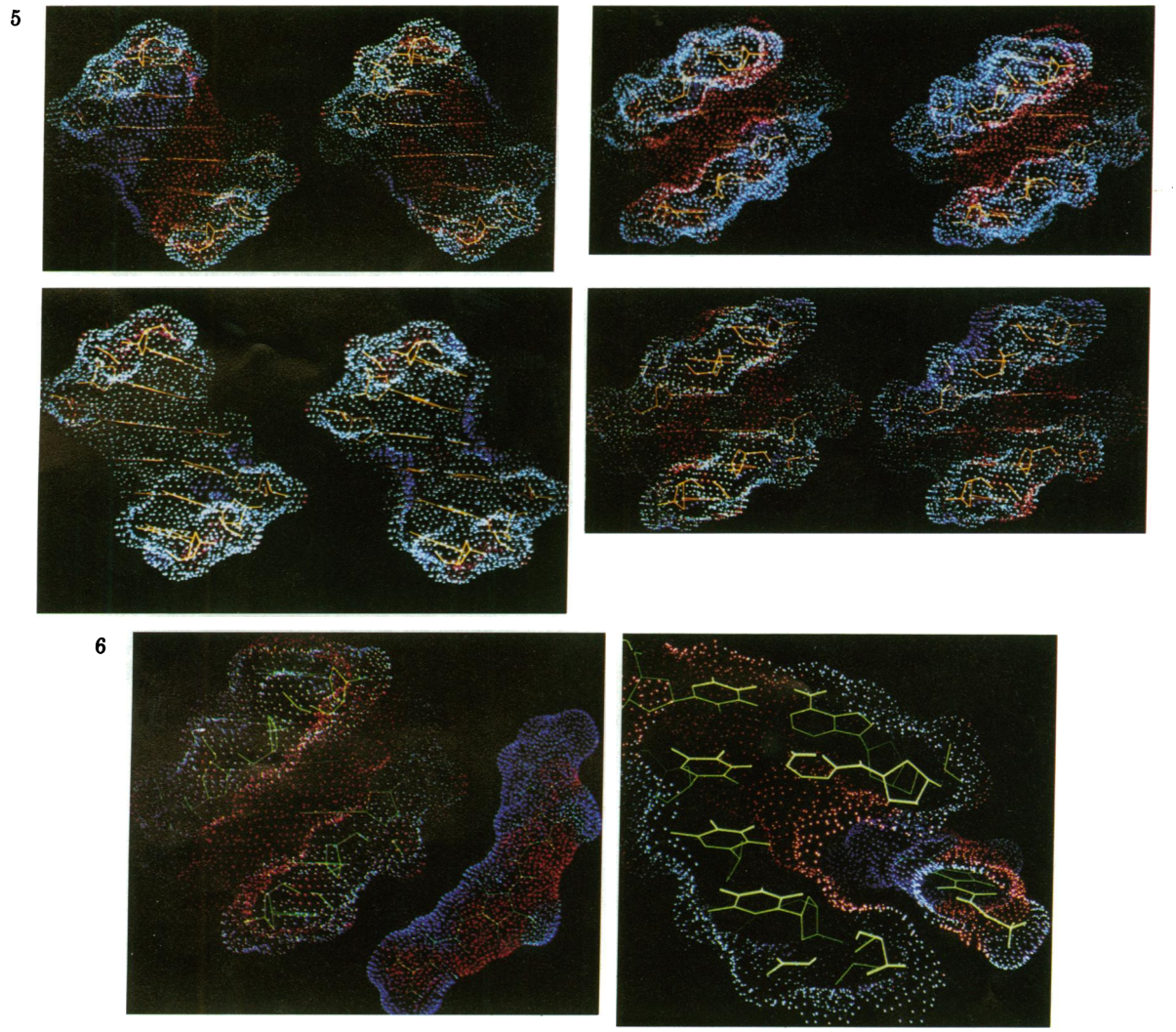

FIG. 5. Electrostatic potential surfaces. Contour levels: red, $V < -4$ kcal/mol; green, -4 kcal/mol $< V < +4$ kcal/mol; blue, $V > +4$ kcal/mol. (*Upper Left*) Major grooves of energy-refined $d(G_6)\cdot d(C_6)$ at left and $d(C\text{-}G\text{-}C\text{-}G\text{-}C\text{-}G)_2$ at right. For $d(G_6)\cdot d(C_6)$, the guanines are on the left and the cytosines are on the right. (*Lower Left*) Major groove of energy-refined $d(A_6)\cdot d(T_6)$ at left and $d(T\text{-}A\text{-}T\text{-}A\text{-}T\text{-}A)_2$ at right. For $d(A_6)\cdot d(T_6)$, the adenines are on the left and the thymines on the right. (*Upper Right*) Minor grooves of energy-refined $d(A_6)\cdot d(T_6)$ at left and $d(T\text{-}A\text{-}T\text{-}A\text{-}T\text{-}A)_2$ at right. (*Lower Right*) Minor groove of energy-refined $d(G_6)\cdot d(C_6)$ at left and $d(C\text{-}G\text{-}C\text{-}G\text{-}C\text{-}G)_2$ at right.

FIG. 6. (*Left*) Electrostatic potential surfaces of netropsin and the minor groove of energy-refined $d(A_6)\cdot d(T_6)$. The blue ridge of netropsin contains the positively charged guanidinium and amidinium groups and has a curvature complementary to the minor groove of the hexanucleotide. Contour levels as in Fig. 5. (*Right*) Cross section of the electrostatic potential surfaces of netropsin and energy-refined $d(A_6)\cdot d(T_6)$ near the postulated optimal complex geometry. Contour levels as in Fig. 5.

a lower affinity, have a T·A pair at base pair 13. This change preserves the polarity of the Watson–Crick hydrogen bond in the major groove but places the purine-N7 lone pair in a different position, which may be a key factor in the relative binding affinities of *cro* protein (which binds strongest to OR3) and λ repressor (which binds strongest to OR1), that determine the control functions of these two proteins.

Earlier studies of protein–nucleic acid interactions (37, 38) and ours agree that a guanine–arginine interaction in the major groove would be unusually strong due to hydrogen bonding and electrostatic complementarity. Our model deemphasizes the importance of A·T pairs (compared to G·C) in the major groove, even though there are amino acid side chains (Asn, Gln) that have hydrogen bonding complementarity to the major groove site of A. Although A·T pair hydrogen bonding interactions are sources of major groove specificity (33), our model suggests that G·C pairs confer greater specificity. Nature likely takes advantage of the greater potential specificity of G·C pairs because there are more than twice as many G·C as A·T pairs in the known recognition sequences of restriction endonucleases (33).

Previous calculations suggest that the global minimum in the electrostatic potential for poly[d(A)·d(T)] occurs in the minor groove, and for poly[d(G)·d(C)] the minimum is in the major groove (39). The electrostatic potential around $d(C\text{-}G\text{-}C\text{-}G\text{-}A\text{-}A\text{-}T\text{-}T\text{-}C\text{-}G\text{-}C\text{-}G)_2$ with fully anionic phosphates leads to surface potentials that are most negative in the central A-A-T-T fragment in both the major and minor grooves (40). This contrasts with our results for phosphate-neutralized $d(C\text{-}G\text{-}C\text{-}G\text{-}A\text{-}A\text{-}T\text{-}T\text{-}C\text{-}G\text{-}C\text{-}G)_2$ in which the most negative minor groove region is the central A-A-T-T but the most negative and most positive regions in the major groove are near the C-G-C-G fragments and in the region between the C-G and A-T sections. This disparity is probably due to the difference in the way the phosphate charges have been modeled. In the earlier model (40) the phosphates were fully charged, but in our model the phosphates have been neutralized. Other recent studies (41, 42) suggest

that electrostatic potential differences between alternating and homopolymer G-C sequences are significant within the grooves, even with $\varepsilon = 1$. Thus, the qualitative electrostatic potential differences among the various sequences presented here are reasonable, although the absolute potentials are rather sensitive to the charge on the phosphates and the dielectric constant.

Netropsin–DNA. Netropsin (II), a basic oligopeptide with antiviral and antitumor activities, binds to the minor groove of A+T-rich DNA (43, 44). The electrostatic potential of this molecule and the minor groove of $d(A_6)\cdot d(T_6)$ are shown in Fig. 6 *Left*. The curvature of the netropsin molecular surface makes it complementary to the minor groove of DNA topographically as well as electrostatically (Fig. 6 *Right*). Netropsin's strong affinity for A+T-rich DNA (44) is probably the result of hydrogen bonding that takes place between the N-H groups of netropsin and the adenine-N3 and thymine-O2 and of the steric complementarity of netropsin with the minor groove. The lower affinity shown for DNA containing G·C pairs (43) is due to the decreased negative potential (44) and the steric effect (20, 45) of the guanine-2-NH_2 group in the minor groove.

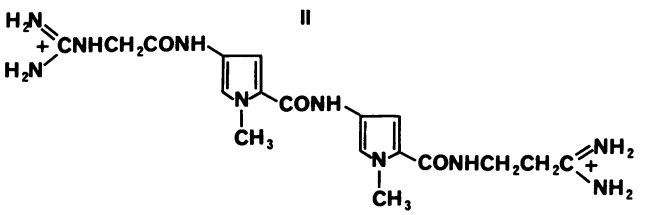

CONCLUSIONS

Hydrogen bonding sites and hydrophobic sites are evident from the electrostatic potential surfaces. In the DNA major groove, proton donors such as NH_2 appear blue (δ^+) and proton acceptors such as N and C=O (δ^-) are shown red. Color coding the surface for electrostatic potential is more general than for hydrogen bond "potential" and delineates cases in which hydrogen bonding is stronger than expected due to the effect of neighboring groups. In modeling hydrophobically driven association, one would attempt to fit the neutral surfaces of the molecules and to minimize the electrostatic mismatches. Electrostatic forces do not necessarily provide the thermodynamic driving force in protein–ligand association, but electrostatic mismatches rarely occur.

Studies of the trypsin–trypsin inhibitor complex demonstrate the striking electrostatic and steric complementarity between the interacting surfaces in a "typical" protein–protein interaction. Consideration of the electrostatic surface potentials of prealbumin and T4 has led to an understanding of the experimental binding data of this protein to thyroid hormone analogs and the failure to detect any binding of DNA to prealbumin. The electrostatic surface potential of DNA is strongly sequence-dependent, with implications for sequence-specific binding of drugs (e.g., netropsin) and proteins (e.g., restriction endonucleases) to DNA.

The computer graphics representation of the molecular surface electrostatic potential is a powerful tool for studying molecular association and may be useful in rational drug design because it facilitates the simultaneous search for both steric and electrostatic complementarity in intermolecular interactions.

We thank Thomas E. Ferrin and Michael Connolly for computer programs and I. D. Kuntz and Daniel Cashman for help and discussion. Photography was by P.K.W. This work was supported by National Institutes of Health Grants RR-1081 (R.L.) and CA-25664 (P.A.K.); J.M.B. is supported in part by the American Foundation for Pharmaceutical Education.

1. Tomasi, J. (1981) in *Chemical Applications of Atomic and Molecular Electrostatic Potentials*, eds. Politzer, P. & Truhlar, D. (Plenum, New York), pp. 257–294.
2. Weinstein, H., Maayani, S., Srebrenik, S., Cohen, S. & Sokolvosky, M. (1975) *Mol. Pharmacol.* **11**, 671–689.
3. Perutz, M. (1978) *Science* **201**, 1187–1191.
4. Warshel, A. (1981) *Acc. Chem. Res.* **14**, 284–290.
5. Hayes, D. M. & Kollman, P. A. (1976) *J. Am. Chem. Soc.* **98**, 3335–3345.
6. Hayes, D. M. & Kollman, P. A. (1976) *J. Am. Chem. Soc.* **98**, 7811–7816.
7. Kollman, P. A. & Hayes, D. M. (1981) *J. Am. Chem. Soc.* **103**, 2955–2961.
8. Perahia, D., Pullman, A. & Pullman, B. (1979) *Theor. Chim. Acta* **51**, 349–357.
9. Sheridan, R. P. & Allen, L. C. (1981) *J. Am. Chem. Soc.* **103**, 1544–1550.
10. Hol, W. G. J., van Duijnen, P. T. & Berendsen, H. J. C. (1978) *Nature (London)* **273**, 443–446.
11. Langridge, R., Ferrin, T. E., Kuntz, I. D. & Connolly, M. L. (1981) *Science* **211**, 661–666.
12. Richards, F. M. (1977) *Annu. Rev. Biophys. Bioeng.* **6**, 151–176.
13. Hopfinger, A. (1973) *Conformational Properties of Macromolecules* (Academic, New York).
14. Gelin, B. & Karplus, M. (1979) *Biochemistry* **18**, 1256–1268.
15. Nuss, M. E. & Kollman, P. (1979) *J. Med. Chem.* **22**, 1517–1524.
16. Kollman, P., Murray, W. J., Nuss, M. E., Jorgensen, E. C. & Rothenberg, S. (1973) *J. Am. Chem. Soc.* **95**, 8518–8525.
17. Dearing, A., Weiner, P. & Kollman, P. (1981) *Nucleic Acids Res.* **9**, 1483–1496.
18. Hayes, D. M. & Kollman, P. A. (1976) *J. Am. Chem. Soc.* **98**, 7811–7816.
19. Bernstein, F. C., Koetzle, T. F., Williams, G. J. B., Meyer, E. F., Jr., Brice, M. D., Rodgers, J. R., Kennard, O., Shimanouchi, T. & Tasumi, M. (1977) *J. Mol. Biol.* **112**, 535–542.
20. Berman, H., Neidle, S., Zimmer, C. & Thrum, H. (1979) *Biochim. Biophys. Acta* **561**, 124–131.
21. Kollman, P., Weiner, P. & Dearing, A. (1981) *Biopolymers* **20**, 2583–2621.
22. Connolly, M. (1981) *QCPE Bull.* **1**, 75.
23. Weiner, P. & Kollman, P. (1981) *J. Comp. Chem.* **2**, 287–303.
24. Adams, D. J. (1979) *Chem. Phys. Lett.* **62**, 329–333.
25. Huber, R. & Bode, W. (1978) *Acc. Chem. Res.* **11**, 114–122.
26. Vincent, J. & Lazdunski, M. (1972) *Biochemistry* **11**, 2967–2977.
27. Blake, C. C. F. & Oatley, S. J. (1977) *Nature (London)* **268**, 115–120.
28. Macleod, K. M. & Baxter, J. D. (1975) *Biochem. Biophys. Res. Commun.* **62**, 577–583.
29. Andrea, T. A., Cavalieri, R. R., Goldfine, I. D. & Jorgensen, E. C. (1980) *Biochemistry* **19**, 55–63.
30. van Jaarsveld, P. P., Edelhoch, H., Goodman, D. S. & Robbins, J. (1973) *J. Biol. Chem.* **248**, 4698–4705.
31. Rask, L., Anundi, H. & Peterson, P. A. (1979) *FEBS Lett.* **104**, 55–58.
32. Drew, H. & Dickerson, R. (1981) *J. Mol. Biol.* **49**, 761–789.
33. Roberts, R. J. (1981) *Nucleic Acids Res.* **9**, 75–98.
34. Smith, H. O. (1979) *Science* **205**, 455–462.
35. Anderson, F. W., Ohlendorf, D. H., Takeda, Y. & Mathews, B. W. (1981) *Nature (London)* **290**, 754–757.
36. Ptashne, M., Jeffrey, A., Johnson, A. D., Maurer, R., Meyer, B. J., Pabo, C. O., Roberts, T. M. & Sauer, R. T. (1980) *Cell* **19**, 1–11.
37. Seeman, N., Rosenberg, J. & Rich, A. (1976) *Proc. Natl. Acad. Sci. USA* **73**, 804–808.
38. Helene, C. (1977) *FEBS Lett.* **74**, 10–13.
39. Pullman, A. & Pullman, B. (1981) in *Chemical Applications of Atomic and Molecular Electrostatic Potentials*, eds. Politzer, P. & Truhlar, D. (Plenum, New York), pp. 257–294.
40. Lavery, R. & Pullman, B. (1981) *Nucleic Acids Res.* **9**, 3765–3777.
41. Dean, P. M. & Wakelin, L. P. G. (1980) *Proc. R. Soc. London Ser. B* **209**, 453–471.
42. Dean, P. M. (1981) *Br. J. Pharmacol.* **74**, 39–46.
43. Zimmer, C., Puschendorf, B., Grunicke, H., Channer, P. & Venner, H. (1971) *Eur. J. Biochem.* **21**, 269–278.
44. Pullman, B. & Pullman, A. (1981) *Stud. Biophys.* **86**, 95–102.
45. Wartell, R., Larson, J. & Wells, R. (1974) *J. Biol. Chem.* **249**, 6719–6730.